

CuSbSe₂ photovoltaic devices with 3% efficiency

Adam Welch^{1,2*}, Lauryn Baranowski^{1,2}, Pawel Zawadzki¹, Stephan Lany¹, Colin Wolden², Andriy Zakutayev^{1*}

¹ National Renewable Energy Laboratory, Golden, CO, USA

² Colorado School of Mines, Golden, CO, USA

*corresponding authors: adam.welch@nrel.gov, andriy.zakutayev@nrel.gov

Recent technical and commercial successes of existing thin film solar cell technologies motivates exploration of next-generation photovoltaic (PV) absorber materials. Of particular scientific interest are compounds like CuSbSe₂, which do not have the conventional tetrahedral semiconductor bonding. Here, we demonstrate 1.5 μm thick CuSbSe₂ PV prototypes prepared at 380-410°C by a self-regulated sputtering process using the conventional substrate device architecture. The p-type CuSbSe₂ absorber has a 1.1 eV optical absorption onset, $\sim 10^5$ cm⁻¹ absorption coefficient at 0.3 eV above the onset, and a hole concentration of $\sim 10^{17}$ cm⁻³. The promising >3% energy conversion efficiency ($J_{sc} = 20$ mA/cm², FF = 0.44, $V_{oc} = 0.35$ V) in these initial devices is limited by bulk recombination that limits photocurrent, device engineering issues that affect fill factor, and a photovoltage deficit that likely results from the non-ideal CuSbSe₂/CdS band offset.

Current thin film solar cell technologies such as CdTe and Cu(In,Ga)Se₂ have achieved champion efficiencies in excess of 20% after decades of research and development, and are being commercialized at a large scale. As such, research and development are free to explore more novel photovoltaic (PV) absorber materials, like Cu₂ZnSnSe₄¹ or Cu₂SnS₃,² both tetrahedrally bonded solids. Such studies of novel inorganic semiconductors can create a more secure energy source by increasing the diversity of the solar energy conversion technologies, with no single chemical element being critical to power generation. In addition, studying non-tetrahedrally bonded PV absorber materials, such as SnS³ and Sb₂Ch₃ (Ch=S,Se)^{4,5}, can reveal which physical properties, chemical characteristics or structural features are most critical for efficient solar energy conversion. For all these reasons, we choose investigate CuSbSe₂ as a PV absorber.

CuSbSe₂ is an interesting novel PV absorber material because it is chemically quite similar to the well-known CuInSe₂, but structurally very different due to the low-valent state of antimony.^{6,7} In CuSbSe₂, antimony is in the +III oxidation state like indium in CuInSe₂; however, unlike indium, antimony contains two lone pair non-bonding electrons that frustrate the tetrahedral bonding, resulting in a layered orthorhombic (space group Pmnb) chalcostybite crystal structure.^{8,9} There has been surprisingly little attention to PV applications of CuSbSe₂, compared to CuSbS₂.^{10,11} The few published studies describe electronic structure (Cu-Se valence band / Sb-S conduction band and $\alpha = 10^4 - 10^5 \text{ cm}^{-1}$)^{12,13}, as well as the optoelectronic properties of thin films ($E_g = 1.1 - 1.2 \text{ eV}$, p-type) and photoelectrochemical device performance ($\sim 10\%$ EQE, $\sim 50 \mu\text{A}/\text{cm}^2$ photocurrent)^{14,15} of Cu-rich and Cu-poor CuSbSe₂ absorbers.

In this letter, we demonstrate initial prototypes of CuSbSe₂ PV devices with a substrate architecture comprised of a CdS front contact and Mo back contact. As previously demonstrated with CuSbS₂,^{16,17} stoichiometric phase-pure CuSbSe₂ can be grown using self-regulated, three-stage approach, where the growth rate is controlled by Cu₂Se flux, while excess Sb₂Se₃ remains in the vapor phase. The resulting micron scale grains grown between 380°C and 410°C have a 1.1 eV optical absorption onset, a hole density of 10^{17} cm^{-3} , $\sim 50\%$ external quantum efficiency, and $>3\%$ energy conversion efficiency in CuSbSe₂. These results are encouraging for a PV device prototype, and call for further research and development of CuSbSe₂ PV technology.

The conditions for absorber synthesis were developed through combinatorial sputtering (see Supplementary information for more details). As shown in Fig. 1, two Sb₂Se₃ binary targets

were oriented perpendicular to a third Cu_2Se source. The glass substrates were intentionally not rotated, resulting in orthogonal gradients of absorber thickness and deposition rate (Fig. 1), since excess Sb_2Se_3 remained in the vapor phase. Normalized to deposition rate, substrate regions closer to the Cu_2Se target experienced a lower Sb_2Se_3 flux than the regions farther from the Cu_2Se target. This relative Sb_2Se_3 flux, ΔF , was quantified as $\Delta F(\text{Sb}_2\text{Se}_3) = cP(\text{Sb}_2\text{Se}_3) / (P(\text{Cu}_2\text{Se}) + \gamma d_t)$, where P are the gun powers, d_t is the throw distance from the Cu_2Se target, γ is a fitting parameter that describes reduction in flux density with increasing throw distance, and c is a constant that converts sputtering power to atom flux (assumed here equal for Cu_2Se and Sb_2Se_3). The resulting CuSbSe_2 absorbers had dense morphology and relatively large ($>1 \mu\text{m}$) but irregular grains (inset, Fig. 2b).

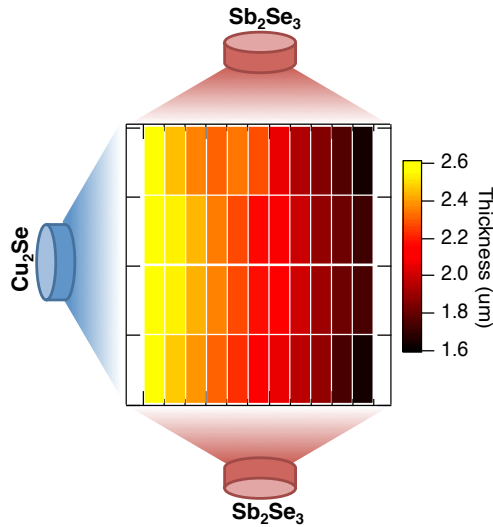


Figure 1: Schematic of the experimental setup showing relationship of sputter sources to substrate, and the resulting XRF measured thickness profile.

The CuSbSe_2 material- and device- combinatorial sample libraries fabricated were characterized using spatially-resolved measurement techniques for composition, structure, thickness and device performance. A total of 44 spatially-resolved automated measurements were taken on each combinatorial sample library, followed by single-point manual characterization of morphology, optical and electrical properties on the most interesting samples. For the absorber materials libraries, 4 equivalent rows of 11 data points were measured, each with different thicknesses, as shown in Fig. 1. For the PV device libraries, 11 equivalent data

points in 4 groups for devices were measured, orthogonal to what is shown in Fig. 1. More fabrication and characterization details for the CuSbSe₂ materials- and device- combinatorial libraries are summarized in Supplementary Information, and were similar to our recent CuSbS₂,^{16,17} and Cu₂SnS₃^{18,19} publications.

Ab-initio calculations were performed using the VASP code,²⁰. The band gap and optical absorption spectrum was theoretically determined from quasiparticle energy calculations in the GW approximation.²¹ In order to determine the single-phase stability regions of CuSbSe₂, we performed density functional theory (DFT) calculations for CuSbSe₂ and the relevant competing phases, including Sb₂Se₃, Cu₃SbSe₃, and Cu₂Se. The respective compound formation enthalpies were determined using the fitted elemental reference energies.²² The vapor pressures of Sb₂Se₃(g) in equilibrium with CuSbSe₂(s) were calculated for the 3CuSbSe₂(s) → Cu₃SbSe₃(s) + Sb₂Se₃(g) and 2CuSbSe₂(s) → Cu₂Se (s) + Sb₂Se₃(g) decomposition pathways. To calculate the free energy change for these reactions we used DFT formation enthalpies of solid phases and the free energy of Sb₂Se₃(s) sublimation calculated from experimental vapor pressure.²³

Previous experimental work by our group^{16,17} has demonstrated phase pure growth of the related CuSbS₂ compound, by employing substrate temperatures above the sublimation of Sb₂S₃ but below the decomposition into Cu-rich phases. The same synthesis strategy has been applied in this work for CuSbSe₂ absorber. As shown in theoretical analysis in Fig. 2a, the shaded yellow region between CuSbSe₂ decomposition and Sb₂Se₃ sublimation defines the processing window for phase-pure material. At a given temperature, there is a range of Sb₂Se₃ equilibrium vapor pressure between the sublimation and decomposition lines for the CuSbSe₂ phase. If the Sb₂Se₃ partial pressure is too high, Sb₂Se₃ impurities will remain in the film. If the Sb₂Se₃ partial pressure is too low, the deposited CuSbSe₂ will decompose to Cu₃SbSe₃. Further reduction in Sb₂Se₃ partial pressure produces no ternary phases. Thus, phase-pure CuSbSe₂ should be grown in the temperature-pressure region bound by these two decomposition lines (Fig. 2a).

Experimentally, the Sb₂Se₃ pressure is controlled in our chamber by the relative Sb₂Se₃ flux (see definition above). Consistent with the theoretical calculations (Fig. 2a), we find that for a given substrate temperature (350C, 380C and 410C in our experiments), there is a range of relative Sb₂Se₃ flux values which produce stoichiometric CuSbSe₂ material with a Cu atomic ratio of Cu/(Cu+Sb+Se)=0.25 (Fig. 2b) and phase-pure XRD pattern (Fig. 3a). The too low relative Sb₂Se₃ flux leads to CuSbSe₂ decomposition into Cu₂Se + Cu₃SbSe₃, resulting in Cu

atomic ratios >0.25 , and too high Sb_2Se_3 flux leads to Sb_2Se_3 impurities remain in the film, resulting in Cu atomic ratios < 0.25 . Projecting experimental Fig. 2b onto theoretical Fig. 2a, it appears that the experimental Sb_2Se_3 relative flux ratios achieved in our chamber roughly translate to an Sb_2Se_3 partial pressure range of $10^{-8} - 10^{-5}$ Torr, depending on the Cu_2Se throw distance. This graded Sb_2Se_3 flux ratio along the combinatorial library results in thicker films and higher Cu chemical potential closer to the Cu_2Se target. Combinatorial studies to decouple these two gradients and to study their effects on CuSbSe_2 device performance are currently in progress and will be reported in a separate full-length article.

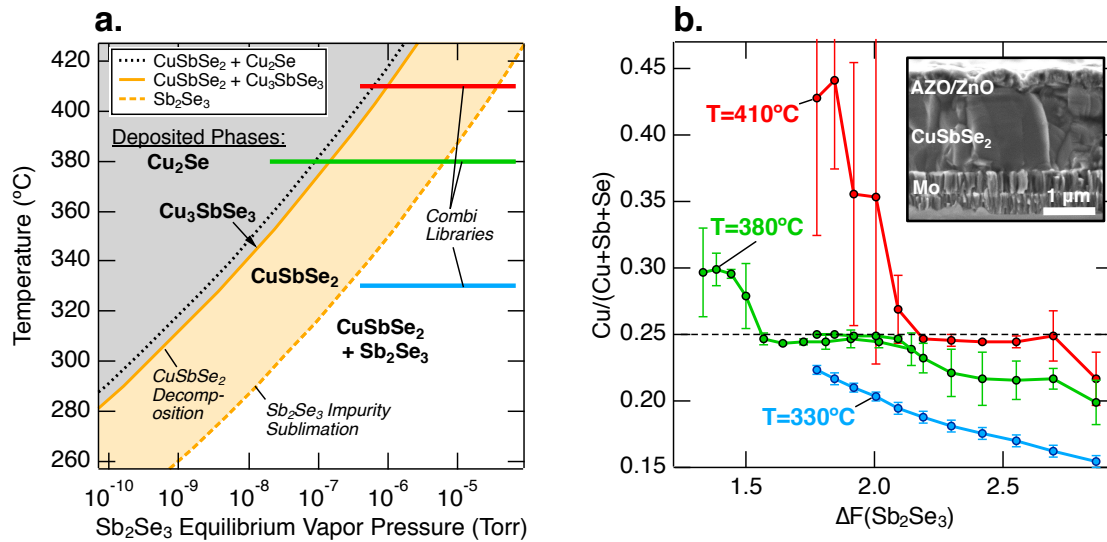


Figure 2: (a) Theoretical calculations reveal a range of Sb_2Se_3 equilibrium vapor pressure and temperature where phase-pure CuSbSe_2 can be grown. (b) Experiments confirm that stoichiometric CuSbSe_2 can be deposited in a range of Sb_2Se_3 fluxes and substrate temperatures. Inset: cross-section SEM image, displaying film thickness, device structure and absorber morphology.

Regions of the combinatorial libraries corresponding to the different amounts of Cu incorporation were characterized for optical absorption to identify the band gap of the phase pure material, and to study the effect of impurity phases on the optical properties. As shown in Fig. 3b, the stoichiometric CuSbSe_2 films had a sharp absorption onset at 1.1 eV that saturated to nearly 10^5 cm^{-1} only 0.35 eV above the band gap. These results are in very good agreement with the GW theoretical calculations, leading to high confidence in the reported CuSbSe_2 optical absorption properties. This is indicative of a nearly-direct band gap in this material, consistent

with the prior theoretical^{12,13} and experimental^{14,15} reports. Cu_2Se impurities appear to increase sub-bandgap absorption in CuSbSe_2 , consistent with additional carriers from this degenerate semiconductor. Conversely, Sb_2Se_3 impurities seem to further reduce sub-band absorption in CuSbSe_2 , possibly due to total elimination of Cu_2Se impurities. However it should be noted that the 10^3 cm^{-1} values are close to the instrument error for the measured very thin $\sim 500\text{nm}$ films, so thicker films would be required to study the sub-gap absorption in more details in the future.

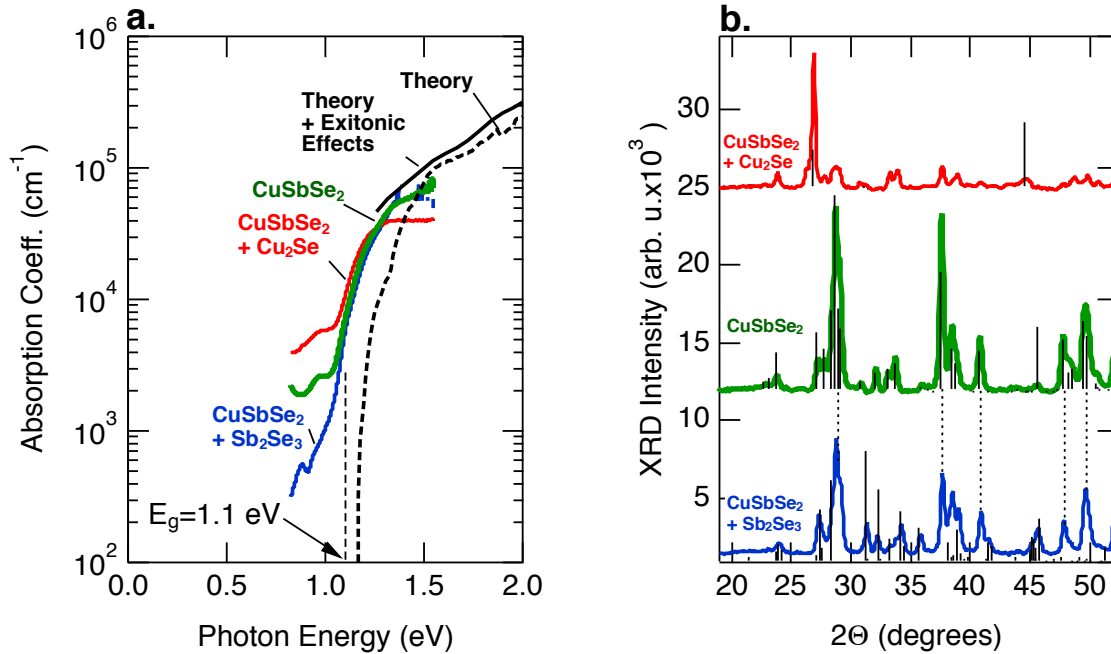


Figure 3: (a) Absorption coefficient values for stoichiometric CuSbSe_2 , and for CuSbSe_2 that contains phase impurities. Black lines are the results of GW theoretical calculations. (b) XRD phase identification for the different regions on the combinatorial libraries. Black lines are the reference patterns for CuSbSe_2 (green), Sb_2Se_3 (blue), and Cu_2Se (red).

Figure 4a displays the JV characteristic of the highest efficiency CuSbSe_2 PV device, along with a histogram analysis of all the nominally uniform, not shunted devices from the thickest ($1.5 \mu\text{m}$) row of a combinatorial library grown at 380°C . Excluding the 2 shunted devices, the 9 remaining devices had average values of: $V_{oc} = 346 \pm 7 \text{ mV}$, $J_{sc} = 20.5 \pm 1.7 \text{ mA/cm}^2$, $\text{FF} = 43.9 \pm 2.8$, and efficiency = $3.12 \pm 0.41\%$. The difference between the J_{sc} measured by J-V (up to 22 mA/cm^2 , Fig. 4a) and integrated EQE \times AM1.5G (up to 18 mA/cm^2 , Fig. 4b) is likely due to asymmetry in the CuSbSe_2 spectral response combined with 400-500 nm peaks in the Xe-lamp spectrum. The thinner ($1.3 \mu\text{m}$) row of devices had slightly lower efficiencies due to lower

photocurrents. The remaining two rows of devices were used for other experiments, and hence are not discussed here.

The J_{sc} , V_{oc} and FF values listed above are approximately a half of what might be expected for an ideal 1.1 eV gap absorber. This is quite promising as for an initial CuSbSe₂ PV device prototype, but calls for further analysis to improve this performance. The less-than-ideal FF is probably due to the lack of device optimization, leading to shunts, isolation issues and so on, which are quite typical of the initial PV device prototypes. The measured non-ideal V_{oc} can be tentatively attributed in part to the extrinsic device problem, namely the likely cliff-type band offset between the n-type CdS heterojunction and the layered ternary CuSbSe₂ absorber (similar to CuSbS₂¹⁷). This is in contrast to tetrahedrally-bonded quaternary Cu₂ZnSnS₄^{24,25} or Cu₂SnS₃^{26,27} where similar V_{oc} deficit is often attributed to the intrinsic materials problem of cation disorder. Finally, the half-of-ideal short circuit currents (J_{sc}) indicate substantial room for improvement in collection of photogenerated charge carriers, given that the 1.5 μm thick CuSbSe₂ layers are not absorption limited (Fig. 3b)

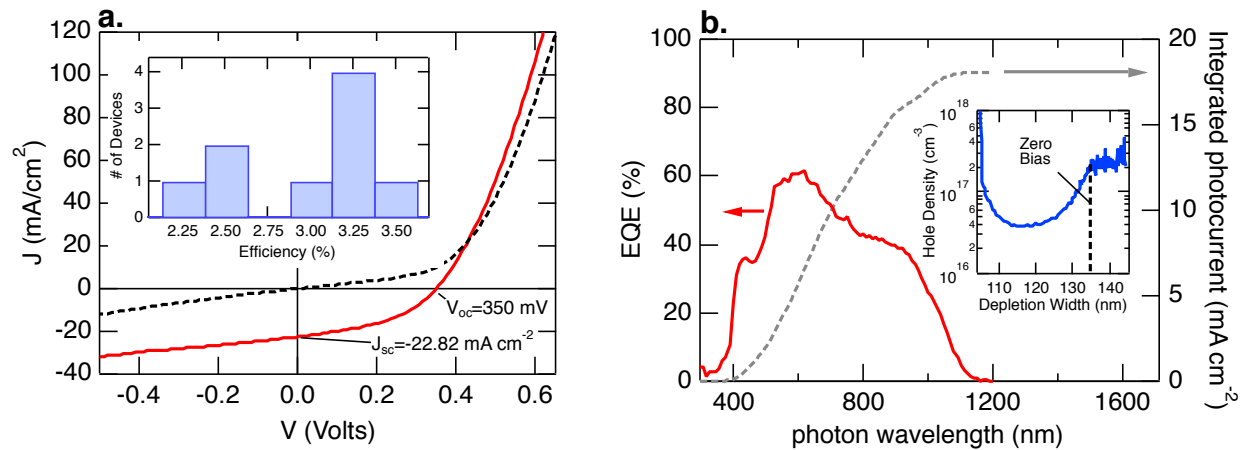


Figure 4: (a) JV results for the most efficient 3.5% CuSbSe₂ PV device and a histogram analysis of efficiency for all 9 nominally equivalent, non-shunted devices from the first row on the combinatorial library as the inset. (b) EQE results for the 3.5% CuSbSe₂ PV device, including the integrated EQE x AM1.5G product, and CV analysis as the inset.

To distinguish between the bulk- and interface photocurrent recombination pathways in the 3.5% CuSbSe₂ PV devices, we performed spectrally-resolved EQE measurement under white light bias (Fig. 4b). As expected, the EQE for > 1000nm and <500 nm is limited by insufficient absorption in CuSbSe₂ and parasitic absorption in CdS, respectively. In the 500 - 1000 nm region

of interest, the EQE results indicate 40% collection between 750 and 1000 nm wavelength, suggestive of significant recombination losses in the bulk. The collection improves up to 60% in the 500 - 750 nm spectral range, pointing to drift-enhanced carrier collection in the space charge region. Consistent with this result, the CV characteristics indicate a narrow depletion width of 135 nm due to relatively high hole concentration of $2 \times 10^{17} \text{ cm}^{-3}$. Given the measured absorption coefficient ($7 \times 10^4 \text{ cm}^{-1}$ at 900nm, Fig. 3a), a Beer-Lambert absorption depth calculation suggest that 50% of the <900nm photons are absorbed within the 135 nm space charge regions. This 50% number is comparable with the average EQE values in the 500-1000 nm spectral range, supporting the hypothesis of drift-enhanced operation of our CuSbSe₂ PV device.

In summary, phase-pure CuSbSe₂ thin films have been synthesized by sputtering, characterized for optical absorption, and made into initial PV device prototypes. The stoichiometric CuSbSe₂ is relatively easy to grow using the self-regulated synthesis technique that keeps excess Sb₂Se₃ in the vapor phase. The CuSbSe₂ absorption onset is indicative of nearly-direct 1.1 eV band gap that matches well the solar spectrum, making this material interesting for thin film PV device integration. Preliminary PV devices in the substrate architecture with Mo back contact and CdS heterojunction partner show promising >3% initial energy conversion efficiencies, limited by bulk photocurrent recombination (affects J_{sc}), likely cliff-type CuSbSe₂/CdS band offset (affects V_{oc}), and device engineering issues (affects FF). Therefore, future work should focus on identification and improvement of band offsets between CdS and CuSbSe₂ to increase V_{oc} , decreasing bulk defect recombination of the CuSbSe₂ absorber material to increase J_{sc} , and usual device engineering improvements to increase the FF.

The “Rapid Development of Earth-abundant Thin Film Solar Cells” project is supported by the U. S. Department of Energy, Office of Energy Efficiency and Renewable Energy, as a part of the SunShot initiative, under Contract No. DE-AC36-08GO28308 to NREL. We would like to acknowledge Clay DeHart for consistent high quality and rapid application of top contact layers, and F. Willian de S. Lucas for informative discussion.

Supplementary information

Absorber synthesis details. For CuSbSe₂ absorber synthesis, we leverage our recently established combinatorial approach to absorber materials research and PV device development, initially demonstrated on the example of the related CuSbS₂ materials. Depositions were

performed in a sputtering chamber with 3×10^{-3} Torr of Ar and 10^{-7} Torr base pressure. The films were grown from 2 Sb_2Se_3 and 1 Cu_2Se targets, each 50 mm in diameter. The absorbers were deposited on 50x50 mm soda lime glass (SLG), or SLG/Mo substrates held at 350-410C during the deposition, and cooled/heated in excess Sb_2Se_3 flux.

Device fabrication details: The CuSbSe_2 PV devices were fabricated by DC sputter deposition of a bilayer Mo on SLG substrates, followed by sputter-deposition of the CuSbSe_2 absorber deposition as described above. The front contact was formed by chemical bath deposition of CdS buffer layer, with subsequent RF sputter deposition of the i-ZnO/ZnO stack and e-beam evaporation of Ni:Al metal fingers and MgF antireflection coating. The devices from contacts were isolated from each other by razor blade scribing.

Characterization details. The resulting combinatorial libraries of the absorber material and PV devices were studied by spatially-resolved characterization techniques, including AM 1.5G J-V measurements of the device performance (calibrated by Si reference cell), X-ray diffraction (XRD) for absorber crystallographic structure and phase composition, x-ray fluorescence (XRF) for absorber chemical composition and thickness (as verified by Dektak profilometer). For several selected points on the libraries we also measured optical absorption properties, cross-section scanning electron microscopy (SEM), external quantum efficiency (EQE), and capacitance-voltage (CV) analysis. Data processing for all tools was done with custom routines implemented in IgorPro software package.

Computational details. The ab initio calculations in this work were performed with the Vienna Ab initio Simulation Package (VASP) using the projector-augmented wave (PAW) implementation of density functional theory (DFT)^{Error! Bookmark not defined.} and many-body perturbation theory in the GW approximation²¹ The Perdew-Burke-Ernzerhof (PBE) generalized gradient approximation (GGA) was used for the DFT exchange-correlation functional²⁸. The GGA+U method²⁹ with $U = 5$ eV was employed to for Cu-d orbitals. The detailed computational settings used for the GW band gap calculations are identical to those published before, including the use of an onsite-potential to account for the underbinding of Cu-d states in GW.³⁰ The optical spectra including excitonic effects were calculation within time-dependent DFT, using a hybrid functional kernel³¹ with a fraction of Fock exchange of $\alpha = 1/\epsilon$, where $\epsilon = 13$ is the static electronic dielectric constant obtained from the GW calculation.

References

- ¹ Lee, Yun Seog, Talia Gershon, Oki Gunawan, Teodor K. Todorov, Tayfun Gokmen, Yudistira Virgus, and Supratik Guha. "Cu₂ZnSnSe₄ Thin-Film Solar Cells by Thermal Co-evaporation with 11.6% Efficiency and Improved Minority Carrier Diffusion Length." *Advanced Energy Materials* (2014).
- ² Umehara, Mitsutaro, Yasuhiko Takeda, Tomoyoshi Motohiro, Takenobu Sakai, Hiroki Awano, and Ryosuke Maekawa. "Cu₂Sn_{1-x}GexS₃ (x= 0.17) thin-film solar cells with high conversion efficiency of 6.0%." *Applied Physics Express* 6, no. 4 (2013): 045501.
- ³ Steinmann, Vera, R. Jaramillo, Katy Hartman, Rupak Chakraborty, Riley E. Brandt, Jeremy R. Poindexter, Yun Seog Lee et al. "3.88% efficient tin sulfide solar cells using congruent thermal evaporation." *Advanced Materials* 26, no. 44 (2014): 7488-7492.
- ⁴ Kim, Dae-Hwan, Sang-Ju Lee, Mi Sun Park, Jin-Kyu Kang, Jin Hyuck Heo, Sang Hyuk Im, and Shi-Joon Sung. "Highly reproducible planar Sb₂S₃-sensitized solar cells based on atomic layer deposition." *Nanoscale* 6, no. 23 (2014): 14549-14554.
- ⁵ Leng, Meiyang, Miao Luo, Chao Chen, Sikai Qin, Jie Chen, Jie Zhong, and Jiang Tang. "Selenization of Sb₂Se₃ absorber layer: An efficient step to improve device performance of CdS/Sb₂Se₃ solar cells." *Applied Physics Letters* 105, no. 8 (2014): 083905.
- ⁶ Kumar, M., & Persson, C. (2013). CuSbS₂ and CuBiS₂ as potential absorber materials for thin-film solar cells. *Journal of Renewable and Sustainable Energy*, 5(3), 031616.
- ⁷ Yu, L., Kokenyesi, R. S., Keszler, D. A., & Zunger, A. (2013). Inverse Design of High Absorption Thin-Film Photovoltaic Materials. *Advanced Energy Materials*, 3(1), 43-48.
- ⁸ Temple, D. J., Kehoe, A. B., Allen, J. P., Watson, G. W., & Scanlon, D. O. (2012). Geometry, Electronic Structure, and Bonding in CuMCh₂ (M= Sb, Bi; Ch= S, Se): Alternative Solar Cell Absorber Materials?. *The Journal of Physical Chemistry C*, 116(13), 7334-7340.
- ⁹ Dufton, J. T., Walsh, A., Panchmatia, P. M., Peter, L. M., Colombara, D., & Islam, M. S. (2012). Structural and electronic properties of CuSbS₂ and CuBiS₂: potential absorber materials for thin-film solar cells. *Physical Chemistry Chemical Physics*, 14(20), 7229-7233.
- ¹⁰ Septina, William and Shigeru Ikeda, Yuta Iga, Takashi Harada, and Michio Matsumura. "Thin film solar cell based on CuSbS₂ absorber fabricated from an electrochemically deposited metal stack." *Thin Solid Films*, 550:700 – 704, 2014.
- ¹¹ Ornelas-Acosta, R. E. and D. Avellaneda, S. Shaji, G.A. Castillo, T.K. Das Roy, and B. Krishnan. "CuSbS₂ thin films by heating Sb₂S₃/Cu layers for pv applications." *Journal of Materials Science: Materials in Electronics*, 25(10):4356–4362, 2014.
- ¹² Kumar, Mukesh, and Clas Persson. "Cu (Sb, Bi)(S, Se)₂ as Indium-free Absorber Material with High Optical Efficiency." *Energy Procedia* 44 (2014): 176-183.

-
- ¹³ Maeda, T., and T. Wada. "First-principles study of electronic structure of CuSbS₂ and CuSbSe₂ photovoltaic semiconductors." *Thin Solid Films* (2014).
- ¹⁴ Colombara, Diego, Laurence M. Peter, Keith D. Rogers, Jonathan D. Painter, and Scilla Roncallo. "Formation of CuSbS₂ and CuSbSe₂ thin films via chalcogenisation of Sb–Cu metal precursors." *Thin Solid Films* 519, no. 21 (2011): 7438-7443.
- ¹⁵ Tang, Ding, Jia Yang, Fangyang Liu, Yanqing Lai, Jie Li, and Yexiang Liu. "Growth and characterization of CuSbSe₂ thin films prepared by electrodeposition." *Electrochimica Acta* 76 (2012): 480-486.
- ¹⁶ Welch, Adam W. and Pawel P. Zawadzki, Stephan Lany, Colin A. Wolden, and Andriy Zakutayev. "Self-regulated growth and tunable properties of CuSbS₂ solar absorbers." *Solar Energy Materials and Solar Cells*, 132(0):499 – 506, (2015).
- ¹⁷ Welch, Adam W., Lauryn L. Baranowski, Pawel Zawadzki, Clay DeHart, Steve Johnston, Stephan Lany, Colin A. Wolden, and Andriy Zakutayev. "Accelerated development of CuSbS₂ thin film photovoltaic device prototypes." *arXiv preprint arXiv:1504.01345* (2015).
- ¹⁸ Zawadzki, Pawel, Lauryn L. Baranowski, Haowei Peng, Eric S. Toberer, David S. Ginley, W. Tumas, Andriy Zakutayev, and Stephan Lany. "Evaluation of photovoltaic materials within the Cu-Sn-S family." *Applied Physics Letters* 103, no. 25 (2013): 253902.
- ¹⁹ Baranowski, Lauryn L., Pawel Zawadzki, Steven Christensen, Dennis Nordlund, Stephan Lany, Adele C. Tamboli, Lynn Gedvilas et al. "Control of doping in Cu₂SnS₃ through defects and alloying." *Chemistry of Materials* 26, no. 17 (2014): 4951-4959.
- ²⁰ Kresse, Georg, and D. Joubert. "From ultrasoft pseudopotentials to the projector augmented-wave method." *Physical Review B* 59.3 (1999): 1758.
- ²¹ Shishkin, M., and G. Kresse. "Implementation and performance of the frequency-dependent G W method within the PAW framework." *Physical Review B* 74.3 (2006): 035101.
- ²² Stevanović, Vladan, et al. "Correcting density functional theory for accurate predictions of compound enthalpies of formation: Fitted elemental-phase reference energies." *Physical Review B* 85.11 (2012): 115104.
- ²³ Piacente, V., P. Scardala, and D. Ferro. "Total vapour pressure of solid Sb₂Se₃." *Journal of materials science letters* 11.12 (1992): 855-857.
- ²⁴ Scragg, Jonathan JS, Léo Choubrac, Alain Lafond, Tove Ericson, and Charlotte Platzer-Björkman. "A low-temperature order-disorder transition in Cu₂ZnSnS₄ thin films." *Applied Physics Letters* 104, no. 4 (2014): 041911.

-
- ²⁵ Schorr, Susan, and Gabriela Gonzalez-Aviles. "In-situ investigation of the structural phase transition in kesterite." *physica status solidi (a)* 206, no. 5 (2009): 1054-1058.
- ²⁶ Zawadzki, Paweł, Andriy Zakutayev, and Stephan Lany. "Entropy-Driven Clustering in Tetrahedrally Bonded Multinary Materials." *Physical Review Applied* 3, no. 3 (2015): 034007.
- ²⁷ Baranowski, Lauryn L., Kevin McLaughlin, Pawel Zawadzki, Stephan Lany, Andrew Norman, Hannes Hempel, Rainer Eichberger, Thomas Unold, Eric S. Toberer, and Andriy Zakutayev. "Effects of disorder on carrier transport in Cu_2SnS_3 ." *arXiv preprint arXiv:1504.01327* (2015).
- ²⁸ Perdew, John P., Kieron Burke, and Matthias Ernzerhof. "Generalized gradient approximation made simple." *Physical review letters* 77.18 (1996): 3865.
- ²⁹ Dudarev, S. L., et al. "Electron-energy-loss spectra and the structural stability of nickel oxide: An LSDA+ U study." *Physical Review B* 57.3 (1998): 1505.
- ³⁰ Lany, Stephan. "Band-structure calculations for the 3 d transition metal oxides in G W." *Physical Review B* 87.8 (2013): 085112.
- ³¹ Paier, Joachim, Martijn Marsman, and Georg Kresse. "Dielectric properties and excitons for extended systems from hybrid functionals." *Physical Review B* 78.12 (2008): 121201.